# Accepted Manuscript

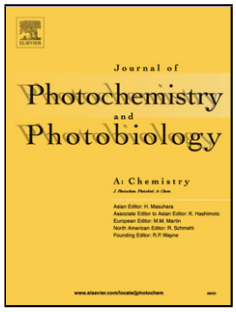


Title: Investigations on the Photo Catalytic activity of Calcium doped $TiO_2$ photo electrode for enhanced efficiency of anthocyanins based dye sensitized Solar cells

Authors: N. Prabavathy, R. Balasundaraprabhu, G. Balaji, A.U. Malikaramage, S. Prasanna, K. Sivakumaran, G.R.A. Kumara, R.M.G. Rajapakse, Dhayalan Velauthapillai

PII: S1010-6030(18)31775-1
DOI: https://doi.org/10.1016/j.jphotochem.2019.03.038
Reference: JPC 11775

To appear in: *Journal of Photochemistry and Photobiology A: Chemistry*

Received date: 5 December 2018
Revised date: 9 March 2019
Accepted date: 24 March 2019

Please cite this article as: Prabavathy N, Balasundaraprabhu R, Balaji G, Malikaramage AU, Prasanna S, Sivakumaran K, Kumara GRA, Rajapakse RMG, Velauthapillai D, Investigations on the Photo Catalytic activity of Calcium doped $TiO_2$ photo electrode for enhanced efficiency of anthocyanins based dye sensitized Solar cells, *Journal of Photochemistry and amp; Photobiology, A: Chemistry* (2019), https://doi.org/10.1016/j.jphotochem.2019.03.038

# Investigations on the Photo Catalytic activity of Calcium doped $TiO_2$ photo electrode for enhanced efficiency of anthocyanins based dye sensitized Solar cells

**N.Prabavathy[*,a,b] praba.snowpearl@gmail.com, R.Balasundaraprabhu[a], G.Balaji[a], A.U.Malikaramage[b,c], S.Prasanna[a], K.Sivakumaran[a], G.R.A. Kumara[d], R.M.G.Rajapakse[c], , DhayalanVelauthapillai[b]**

*[*,a]Centre for Surface Science, Department of Physics, PSG College of Technology, Coimbatore, INDIA*
*[b]Faculty of Science and Engineering, Western Norway University of Applied Sciences, Bergen, NORWAY.*
*[c]Department of Chemistry ,University of Peradeniya, Peradeniya, SRI LANKA.*
*[d]National Institute of Fundamental Studies, Kandy, SRI LANKA.*

**[*]Corresponding Author: phone: 0422-4344535**

**Graphical abstract**

## Highlights

- Ca doped $TiO_2$ nanorods have been prepared using hydrothermal method.
- Anthocyanin pigments from natural rose petals is used as a sensitizer
- Field Emission scanning electron Microscopy revealed the morphological change of nanorods to nanospikes after doping.
- Optical studies revealed higher absorbance spectra for 3% Ca - doped DSSC and band gap reduced from 3.10 eV to 2.75 eV
- Usage of UV filters reduces the incident photon conversion efficiency in undoped DSSC by 10%.
- The photovoltaic conversion efficiency of 3% Ca doped DSSC sensitized by rose dye is 2.32% due to the passivation of Photocatalytic activity in $TiO_2$ photo electrode.

**Abstract:**

The rich photo catalytic activity (PCA) of $TiO_2$ deteriorates the photovoltaic performance of natural dye sensitized solar cells (DSSC) on irradiation. To improve the stability of natural dye in DSSC,

the PCA of $TiO_2$ must be passivated or reduced, without affecting the electron transfer kinetics. UV filters can be employed to avoid the direct band gap excitation in $TiO_2$. But the blocking of photons in UV region decreases the Incident Photon to current Conversion Efficiency (IPCE) of the solar cell. Taking this factor into consideration, virgin and calcium (1%, 2%, 3%, 4% and 5%) doped $TiO_2$ photo electrodes were grown by one step hydrothermal method on Fluorine doped Tin Oxide (FTO) substrates. The structural, morphological and optical properties of Ca doped nanorods passivate the free electrons on the $TiO_2$ surface, thereby minimizing the PCA in the film. The 3% Ca doped $TiO_2$ nanorods exhibited higher resistance to PCA when compared undoped $TiO_2$ photo electrode. This increased the photovoltaic conversion efficiency of rose dye sensitized DSSC to 2.32%.

**Key words**: Ca- doping, $TiO_2$ nanorod, Nanospike, Rose dye, Dye sensitized solar cells, Photo catalytic activity, Hydrothermal method.

## 1. Introduction

Natural dyes can be effectively used as sensitizers for dye sensitized solar cells (DSSC). The cost and the preparation of natural dyes are cheaper and easier than synthetic dye such as Ruthenium [1]. However the efficiency obtained using the natural dyes for DSSC is rather low, due to their instability in invitro condition. The main cause for the instability of natural dye is the high photo catalytic activity (PCA) of photo electrode in DSSC [2]. Many results reported in the literature have concentrated on increasing the PCA of $TiO_2$ for enhancing the conduction of electrons in DSSC [3]. However, $TiO_2$ is a superior photo catalyst and is effectively used for photo catalytic dye degradation [4]. The photo catalytic activity (PCA) of $TiO_2$ releases electrons on the surface of the film on absorbing sunlight in the UV region. The free electrons on the surface readily react with the atmosphere and produces free radicals. These radicals in turn destroy the organic matter present nearby such as a natural dye. In case of DSSC, the natural dye sensitized on the $TiO_2$ is destroyed by the free radicals. This decreases the efficiency of DSSC after few seconds of irradiation. The use of UV filters can substantially reduce the degradation of solar cell by blocking the photons with energy equal to the wavelength of light in the UV region. The number of photons entering has direct impact on the Light Harvesting efficiency (LHE) in the solar cell. In a work by Carnie et al [5], it has been observed that, the use of filters in DSSC have reduced the photovoltaic performance of the cell due to low electron density available for the electron transfer. Therefore tuning the components of DSSC, to passivate the PCA will help in improving the efficiency of solar cell with good stability. The effect of PCA on DSSC is discussed detail in the later section.

Anthocyanins, a flavonoid pigment extracted from rose petals are used as natural sensitizer for the fabrication of DSSC. They show a broad absorption spectrum in the visible region and the presence of carboxyl group helps in anchoring with $TiO_2$ molecules for good sensitization in DSSC [6]. They are also intrinsically rich with antioxidants. The antioxidant scavenges the free radicals generated because of PCA in photoelectrode in DSSC to a smaller extent. This also becomes an additional advantage for employing them in DSSC. Citric acid is used as solvent for the extraction of anthocyanins from rose petals based on our previous work [7] for higher anthocyanin content and maintaining color stability for a longer period.

The PCA of photoelectrode in DSSC can be further passivated to an extent by synthesizing a stable polymorph and modifying the film characteristics by adding a suitable dopant. The photo electrode can be prepared by various techniques such as sol gel method [8], hydrothermal method [9], solvothermal method [10], microwave method [11], electro deposition [12], electrospinning [13] and Spin – Silar [14] . $TiO_2$ exists in three polymorphs- anatase, rutile and brookite (amorphous). The rutile phase is the stable phase among all other polymorphs of $TiO_2$. The anatase and rutile phase of $TiO_2$ are characterized by the oxygen vacancies and intrinsic defects in the crystal structure [15]. The oxygen vacancies readily act as trap centres for free electrons generated during photo induced reaction. This slowly reacts with moisture and enhances the PCA as compared to rutile $TiO_2$ phase.

Generally, the anatase phase of $TiO_2$ is synthesized at low temperature and on annealing the $TiO_2$ to higher temperature yields the most stable rutile phase. But in hydrothermal method, the increase in pressure increases the volume of crystal formed on the substrate and reaches a state of a compact stable structure (Rutile phase) even at low temperatures [16]. The hydrothermal method is also used to produce 1D nanostructure such as $TiO_2$nanorods, nanotube and nanofiber. The nanorods provide a direct electron transfer to reduce electron recombination and good porosity for dye adsorption [17][18]. Hence in this work, $TiO_2$nanorods with pure rutile phase have been prepared as photo electrode for DSSC by hydrothermal method at a working temperature of $180^o$ C. To study the effect of PCA of photo electrode in the DSSC using natural dyes, it is varied by doping the $TiO_2$nanorods with a suitable dopant concentration.

Doping influences the band structure of $TiO_2$ and causes changes in the properties such as charge transport, recombination kinetics and PCA [19]. Alkali earth metals such as calcium (Ca) and sodium (Na) are widely used as mordants for dye fixation in fabric. Similarly, Weixin Li et al [20] have doped Ca on $TiO_2$nanorodsfor DSSC using ruthenium as sensitizer and observed that the Ca doping has increased the photovoltaic performance of the cell due to increase in dye concentration in the photo electrode.

In the present work, Ca is used as a dopant element for increasing the dye concentration and monitoring the PCA in the photo electrode. Increasing the percentage of Ca doping has influenced morphological and electronic changes in the photo electrode that contributes for the increase in DSSC performance to an efficiency of 2.32%. The obtained efficiency is 1.6 times higher than our previous work [21]. The performance of DSSC with UV filter is also experimented in this work to signify the importance of PCA passivation. The photo catalytic activity of rose dye in presence of Ca doped $TiO_2$ films has been investigated and reported for the first time in this work.

## 2. Experimental details

Titanium isopropoxide (TTIP, 97%), conc HCl (36%), ethanol, acetone, calcium chloride and citric acid were used. Fluorine doped Tin Oxide (FTO) plates having 7 Ω as sheet resistance was used.

### 2.1. Synthesis of undoped and Ca-doped $TiO_2$ nanorods.

The $TiO_2$ nanorods were prepared by hydrothermal method and details of it are reported elsewhere [21]. Equal proportion of distilled water and conc. HCl were taken in a beaker and mixed for an hour by magnetic stirrer. 0.5 ml of TTIP was added drop wise to the above solution and stirred for an hour. After stirring, the solution was transferred to a teflon lined stainless steel autoclave (50 ml). The pH of the initial solution was maintained at 1. FTO substrates were placed vertically along the wall of the autoclave such that the conducting side faces towards the solution that creates more nucleation sites for the rod growth. The autoclave was then sealed and heated in a muffle furnace at $180^{\circ}$ C for 4 hours. Thereafter, autoclave was allowed to cool to room temperature. FTO substrates were then removed from the autoclave and washed several times with distilled water to remove impurities in the film if any. A thin uniform white layer coating on the FTO substrates confirm the presence of $TiO_2$. To improve the crystallinity, the $TiO_2$films are annealed at $450^0$C for 30 mins.

To prepare Ca doped $TiO_2$ nanorods, different amounts of $CaCl_2$ (1%, 2%, 3%, 4% and 5% by weight) is dissolved in the precursor solution additionally to the above procedure. As the concentration of Ca increased to 5%, it resulted in the peeling of $TiO_2$ layer from the FTO substrates. Hence 1%, 2%, 3%, 4% of Ca is considered for the experimental work. The pH of the precursor solution remained 1 on addition of $CaCl_2$ from 1% to 5%. Undoped $TiO_2$ film, 1% Ca doped $TiO_2$, 2% Ca doped $TiO_2$, 3% Ca doped $TiO_2$ and 4% Ca doped $TiO_2$, are labeled as UD, D1, D2, D3 and D4 respectively.

### 2.2. Extraction of anthocyanin dye from rose petals

The preparation of dye is followed from our previous work [7]. 10g fresh flowers of *rose* petals were taken in a container and 10 ml of citric acid solution (1g/100ml) is introduced in the container. The petals were gently pressed in the solvent by a glass rod for good concentration. The containers were stored in dark for one day as the presence of light disturbs the solvent effect. The extract is again used as solvent for extracting the dye from fresh rose flowers. This improves the concentration of rose dye and the extract is stored in an amber bottle and refrigerated at 4˚C.

### 2.3. Sensitization of $TiO_2$ film

The synthesized undoped and doped $TiO_2$ nanorod films were treated with the algal buffer layers as reported elsewhere [21]. The Buffer layer treated films were sensitized by immersing them in a beaker containing rose extract individually. This was maintained at room temperature in a dark room for 24 hrs. Then the films were taken out and the excess dye was removed with ethanol.

### 2.4. Fabrication of DSSC

The sensitized doped and undoped $TiO_2$ films are sandwiched with a platinum electrode (with holes) and sealed with surlyn ionomer (25µm thick). The liquid iodine/iodide electrolyte is introduced in the air gap of films through the holes in the platinum electrode. And the hole is sealed with a cover slip. The effective area of solar cell is 0.814 $cm^2$.

## 3. Characterization studies

The crystalline phase of $TiO_2$ nanorods were analyzed using X-ray diffractometer (XRD, SHIMADZU LabX-6000) with a Cu target (λ=1.5409 Å). The samples were scanned with 2θ values ranging from 10° to 80°. The angles of the characteristic peaks were measured from the plot and indexed by using JCPDS data. The shape and size of the synthesized nanorods with EDAX were analyzed using field emission scanning electron microscopy (FE-SEM, ZEISS, SIGMA, UK). X-ray photoelectron Spectroscopy (XPS) studies were carried out using ESCA2000 (VG microtech: UK). Absorbance and dye concentration of the films was recorded using a JASCO UV VIS NIR (Model V770) spectrophotometer operating at a resolution of 2 nm. High resolution transmission electron microscope (HRTEM) images of the prepared samples. The Photo Catalytic Activity measurements were measured using a UV- A source lamp and the concentration dye is calculated using spectrophotometer. Photoluminescence spectra were recorded in PerkinElmer LS 45 Fluorescence Spectrometer. The IPCE measurement was measured in PEC- S20 .Table Top solar simulator PECELL- L01 is used for IV measurements. UV filter of wavelength cut off 417 nm was used to measure the DSSC (with UV filter).

## 4. Results and Discussion

### 4.1. Structural analysis

The crystalline phase of undoped and doped $TiO_2$ films was confirmed by the XRD studies. Figure 1 shows the XRD plot of undoped and Ca-doped $TiO_2$ nanorods. The peak position at (110) (130) (111) (200) (220) (150) (240)(151) (002) (310) clearly states that the $TiO_2$nanorods exhibit single stable rutile phase in accordance with JCPDS No : 530619 [7]. The lattice mismatch between the FTO substrates and the $TiO_2$ crystals deposited on them have influenced the growth of $TiO_2$nanorods vertically to the substrate in (110) plane [22]. No other phases of anatase and brookite were observed. The significance of rutile phase of $TiO_2$ over the photocatalytic activity in DSSC has been discussed elaborately in our previous work [2].

The XRD pattern of Ca doped $TiO_2$nanorods shows greater crystallinity compared to the undoped nanorods. The doping of Ca on to the $TiO_2$ crystal structure effectively takes place by the substitution of $Ca^{2+}$ions (ionic radius = 0.99 Å) in place of $Ti^{4+}$ ions (ionic radius = 0.61 Å) in the crystal lattice [23].This causes stress in the lattice which is explained by the shifting of peaks towards lower 2θ values [24]. The 4% Ca doped $TiO_2$ (D4) shows a shift in the peak and confirms the substitution of $Ca^{2+}$ atom in the $TiO_2$ lattice. Whereas the lower doping percentage of Ca in the $TiO_2$ structure (D1, D2 and D3) doesn't display any peak shift but the intensity of peaks have increased. This shows good crystallinity on increased doping and the calcium atoms must have occupied the surface states without disturbing the crystal lattice [25].

Also from the XRD analysis, the average crystallite size and strain of the films were obtained and tabulated in Table 1. The average crystallite size (t) was calculated using the Debye-Scherer formula.

$$t = \frac{k\lambda}{\beta \cos\theta} \quad \textbf{(1)}$$

where the constant *k* depends upon the structure of the crystallite (here, k=0.94), $\lambda$ is the wavelength of X-rays used (CuKα: 1.5405 Å), ?? is the full width at half maximum of diffraction peaks and θ is the angle of diffraction. The strain was calculated using Williamson - hall Plot using. It is plotted with sin θ on the x-axis and β cos θ on the y-axis (in radians). A linear fit for the plot extracts the particle size and strain from y-intercept and slope respectively. It is observed that the crystallite size decreases for D4 and also it suffers more strain compared to UD, D1, D2, and D3 due to the higher Ca dopant concentration that might have induced structural changes in the lattice.

### 4.2. HRTEM

Figure 2 shows the TEM image of undoped and 3% Ca doped $TiO_2$ nanorods. Figure 2 (a,b,c) and Figure 2 (d e, f) respectively, shows the lattice fringe pattern and the SAED pattern of hydrothermally grown undoped and Ca doped $TiO_2$nanorods. The TEM image in Figure 2 (a) clearly shows that a single rod is made up of a bunch of smaller rods. The kinetics of nucleation and growth of nanorods are detailed in the later section. The interplanar spacing for undoped nanorods $d_{210}$= 0.306 nm clearly corresponds to the rutile phase of $TiO_2$. In Figure 2 (d), it can be observed that the rods form sharp edges in the form of spikes facing all directions. The morphological change is caused because of Ca doping in the $TiO_2$ film. The interplanar spacing for doped nanorods yields a value of $d_{200}$= 0.326 nm that also confirms the rutile phase of nanorods.

### 4.3. Morphological analysis

The surface morphology of undoped and Ca doped $TiO_2$ nanorods with FESEM and their corresponding cross sectional images are shown in Figure 4. The morphology of the rods is changed by increasing the concentration of Ca-dopant in the precursor solution. No significant change has been observed in the rod morphology for the 1% Ca dopant concentration (Figure 3(d,e,f)) . On increasing the concentration of doping to 2% (Figure 3(g,h,i)), the rectangular shaped rods gets agglomerated and results in a cone shaped structure. Further increase in dopant concentration of Ca to 3% (Figure 3(j,k,l)) results in spike shaped nanorods. The nanospikes start breaking on increasing the concentration to 4% (Figure 3(m,n,o)), which might reduce the performance of the film for the direct transfer of electrons. The nanorod spikes observed in the 3% Ca dopant might increase the scattering phenomena thereby enhancing the absorbance in the film. It is also observed that the surface area of the film can be increased by increasing the length of nanorod [27]. From the FESEM results, the length of nanorods is found to increase from 2.26 µm (UD) to 2.77 µm (D3) for increase in dopant concentration. This promotes $TiO_2$ film with high surface area and enhances the dye adsorption in the film. But the length of rods decreases to 2.5 µm (D4) for 4% dopant concentration due to the breakage of nanorods in the film that hinders the direct electron transfer in the film.

#### 4.3.1. Mechanism and kinetics of rod formation in undoped and doped $TiO_2$ films

Conc HCl and distilled water are mixed in equal proportion in a beaker. The solution is maintained at pH 1. A few drops of TTIP are added to the above solution. This produces a supersaturated solution that initializes the nucleation of crystals. At an optimum temperature and pressure, the strong acidic nature of HCl acts as a catalyst in driving the hydrolysis reaction of TTIP, which produces hydrated Titanium hydroxide species [28].

$$\boldsymbol{Ti(OR)_4 + 4H_2O \rightarrow Ti(OH)_2 + 4ROH} \quad \textbf{(2)}$$

This is condensed further to form $TiO_2$ molecules (nucleus). When the initially formed, nucleus reaches the critical size, they form an initial seed layer on the FTO substrates immersed in the solution, otherwise they get soluble in the solution and the reverse reaction proceeds.

$$\boldsymbol{Ti(OH)_2 \rightarrow TiO_2.xH_2O + (2-x)H_2O} \quad \textbf{(3)}$$

Generally, there are two common type of nucleation that takes place in a substrate - surface nucleation and grain boundary nucleation [29]. The FTO substrates act as a matrix for the seed nucleation. The nucleus formed in the solution, deposits on the grain boundaries of FTO at first, preferably due to lattice mismatch sites. The nucleus takes the spherical shape due to the lower surface energy. The seed tend to grow (nanocrystals) as a result of Ostwald ripening (OR) mechanism [28]. It is a diffusion-limited growth of nanomaterial at the expense of smaller ones. Simultaneously, the nanocrystals undergo oriented attachment (OA) mechanism (i.e. the particles with same crystallographic orientations collide to form a stable structure) and grows into a single nanorod. The intensity of rods in the grain boundaries increases as time increases. Hence the rods themselves arrange in an oblique way to minimize the surface energy and become thermodynamically stable. Figure 4 shows that each rod is made up of a bunch of smaller rods. This explains the OR and OA in the nanocrystal growth. The cause for rectangular dimension of nanorods at the tip end and the morphological changes because of doping is also illustrated in the Figure 4.

$CaCl_2$ is introduced as a dopant source in amounts of 1%, 2%, 3%, 4% and 5% by weight to the initial precursor solution. As the enthalpy of formation of $Ca^{2+}$ ions is greater (because of higher lattice energy) compared to $Ca^{+}$ ions, the $CaCl_2$ dissociates to give $Ca^{2+}$ ions and 2 moles of HCl [28].

$$\boldsymbol{CaCl_2(H_2O)_x \rightarrow Ca^{2+} + 2HCl} \quad \textbf{(4)}$$

$$\boldsymbol{TiO_2 + Ca^{2+} \rightarrow Ca - TiO_2} \quad \textbf{(5)}$$

This further makes the solution acidic. The interference of $Ca^{2+}$ ions alters the morphology of nanorods. The tail of nanorods decreases as the $Ca^{2+}$ ions concentration increases from undoped to 4%.

But, at 3% (D3) and 4% (D4) $Ca^{2+}$ concentration, the surface nucleation predominates, hence nucleus spreads all over FTO, which grows and forms nanospikes in all direction (nanospike ball) on the surface of FTO. The $Ca^{2+}$ ions must have accumulated on the tail of nanorods that would have restricted the deposition of $TiO_2$ molecules and finally appearing a cone shaped spike structure. The nanospikes have distinguished characteristics of playing as a scattering layer for maximum light absorbance in the $TiO_2$ film [30]. The nanospikes that are formed at 4% $Ca^{2+}$ concentration are not stable. They are all broken and scattered all over the film that decreases the light absorbance, which can be visibly observed from the absorbance spectra.

### 4.4. EDAX Analysis

The EDAX spectra and mapping of elements of undoped (UD) and 3% Ca doped nanorods (D3) are shown in Figure 5. The weight % and atomic % of the elements present are tabulated in the inset. A titanium atom bonds with two atoms of oxygen to form a stable molecule [26]. The atomic percentage ratio of Ti:O in the EDAX shows a stochiometric stable molecule formation. The Ca presence in the 3% Ca doped $TiO_2$ film (D3) is confirmed by the EDAX spectra with wt % of 3.08. This shows the effective incorporation of Ca atoms on the surface of $TiO_2$ films. The EDAX Mapping shows the distribution of elements present in the film for UD and D3 films. The Ca atoms are evenly distributed for D3 all over the surface.

### 4.5. Optical Studies

The Optical properties of the $TiO_2$ films were studied using UV- Visible spectroscopy. The inset figure in Figure 6(a) shows the absorbance spectra of samples UD, D1, D2, D3 and D4 with sodium alginate buffer layer. The absorbance peak in the UV range of 200 nm to 400 nm for $TiO_2$ films confirms the formation of $TiO_2$ molecules. The intensity of absorbance peak increases on increasing the Ca dopant concentration to 3% but starts decreasing on higher dopant concentration of 4% (D4). Incorporation of Ca atoms in the $TiO_2$ films changes the morphology of $TiO_2$ film from nanorods to nanocones and then to nanospikes [31]. This results in enhancing the light scattering in film which helps in absorbing maximum light. On increasing the dopant concentration to 4%, the spikes starts collapsing and reduce the light scattering in the film, which results in lower absorbance of sunlight in the UV range. Figure 6 (a) shows the Tauc plots of the $TiO_2$ films, which on extrapolation yield the energy band gap. The $TiO_2$ conduction

band edge shifts towards longer wavelength on increasing the dopant concentration from 1% to 3% giving band gap values from 3.1 eV for UD to 2.75 eV for D3. But the band gap for D4 starts increasing to 3.19 eV, which is due to the decrease in particle size in the film [32]. It is observed that the structural, morphological and optical properties of 4% Ca doped DSSC differs from the other films. This can be explained by the effective doping of Ca on the lattice of $TiO_2$ molecules that cause more strain in the structure which contributes for the different behavior as seen in Table 1. Figure 6 (b) shows the absorbance spectra of rose sensitized $TiO_2$ films with spirulina buffer layer. The broadening of peak in the visible range confirms the sensitization of dye molecules on the $TiO_2$ film [33].

The dye adsorption on the surface of $TiO_2$ film is studied by measuring the dye concentration in the film. The dye absorbed on the film is measured by desorbing the sensitized films in a solution of NaOH in water/ ethanol (1.0 M, 50:50, v/v) [34]. The dye concentration is then calculated by UV visible spectrophotometer. Table 2 details the dye concentration of Ca-doped and undoped $TiO_2$ sensitized by rose dye. The dye concentration in the $TiO_2$ film increases with Ca concentration but decreases for 4% Ca concentration. It might be due to the low surface area available for dye adsorption due to the aggregation of particles.

### 4.6. XPS Analysis

The elemental composition of the films can be studied using X-ray Photoelectron Spectroscopy (XPS). Figure 7 (a) shows the survey spectrum of annealed undoped (UD) and Ca doped $TiO_2$ (D3) films. The presence of individual elements Ti, O and Ca (in D3) could be observed in the spectrum. Further the survey spectrum reveals the presence of C 1s at 285.29 eV. The obtained binding energy has a 0.5 eV shift from the standard XPS value [35]. This is due to carbon contamination in the film from the atmosphere that causes a 0.5 eV shift for all other individual elements.

Figure 7 (b) shows the core level spectra of Ti. It is observed that the Ti $2p_{1/2}$ and Ti $2p_{3/2}$ orbitals have their maximum peaks at 464.80 and 459.06 eV. The oxidation state of the Ti atom in the film can be calculated from the difference in the maxima of the Ti doublet states [36]. From Figure 7 (b) the difference of maxima of Ti 2p orbitals yields a binding energy value of 5.72 eV, which confirms the presence of Ti in +4 oxidation states [37]. This confirms the oxide formation in the film from the XPS spectra.

The Oxygen spectrum in Figure 7 (d) defines a maximum peak at binding energy 530.46 eV for samples UD and D3. This definite peak corresponds to O1s orbital. The peak also includes a shoulder bound at higher binding energy. The deconvolution of the major peak gives peak i, ii respectively as shown in Figure 7 (e). The peak i corresponds to binding energy value 532 eV. It is due to the O-H species on the surface. The peak ii corresponds to the energy value 530.3 eV. It is due to the hydroxide bonding with Ti atoms and C-O-C or C-OH groups from the oxidized carbons adsorbed on the surface[38]. At this phase, the shoulder bound of O1s peak increases as surface defect increases rapidly with increase in temperature. These defect sites forms a perfect place for water dissociation and the molecules are stabilized on the surface at higher temperature. This also helps in analyzing the $TiO_2$ crystal structure[39]. The lower shoulder in Figure 7 (d) reveals the presence of rutile phase in the $TiO_2$ film due to lower surface defects [40]. From the survey spectrum for D3 film, the presence Calcium is confirmed. Figure 6(c) shows the Ca 2p peaks with binding energy value 351 eV and 347 eV for Ca $2p_{1/2}$ and Ca $2p_{3/2}$ orbital's respectively.

From the survey spectrum the composition of the individual element is determined by the area under the peak divided by its Relativity sensitivity factor (RSF), which is further divided by the sum of all the elements divided by their respective RSF [41]. Table 3 shows the relative elemental percentage of the films UD and D3. The proportion of Ti:O atoms are in the ratio 2:1 for UD and D3 , this gives an uniform stoichiometry of the $TiO_2$ film formed on the sample surface.

Figure 8 (a) shows the VB spectra of UD and D3 films. The UD and D3 show a Valence band maximum ($E_{VBM}$) of 2.26 eV and 0.60 eV respectively. Doping influences a shift in the ($E_{VBM}$) that alters the consecutive band levels as shown in Figure 8 (b) [42]. The scale in figure 8 (b) depicts the energy levels in NHE. It can be observed that the decrease in $E_{VBM}$ in D3 due to doping, shifts the conduction band maximum ($ECB_{max}$) to higher energy level [43]. The band gap of undoped and Ca doped $TiO_2$ is obtained from the Tauc plot as in Figure 6 (a). This favors electron injection feasible at a higher rate for D3 compared UD, which directly influence the photovoltaic efficiency in DSSC.

### 4.7. Photocatalytic Activity Measurements (PCA)

In water treatment processes, removal of toxic organic dyes using semiconductors is promising. $TiO_2$ is the widely used semiconductor for the degradation of dyes under visible light [44]. The extent of photocatalytic activity depends on several factors: pH and initial concentration of dyes; morphology, phase and the concentration of $TiO_2$ particles[45]. For DSSC, the photocatalytic degradation of natural dyes must be reduced to improve the efficiency and stability of cells. The dye degradation efficiency decreases on improving the concentration of the initial dye solution. Hence, the concentration of rose dye

was improved by following the extraction procedure in the experimental section. When the pH of the dye solution is more acidic, it enhances the degradation. The pH of the rose dye solution was maintained at pH 3 by using citric acid as solvent. The anatase phase of $TiO_2$ is likely to be more probable to photo degradation compared to rutile phase of $TiO_2$ [46]. Also the morphology of $TiO_2$ particles plays an important role in the photocatalytic degradation of dye. The PCA is a surface based mechanism; it increases with increase in the surface area of $TiO_2$ nanoparticle. Since the $TiO_2$nanorods have lower surface area compared to nanoparticles, the PCA is limited to an extent in the as prepared rutile $TiO_2$nanorods (UD) compared to anatase phase $TiO_2$ film. The mechanism of photocatalytic degradation of organic dyes is explained in detail below. Figure 8 explains the mechanism of PCA of $TiO_2$ in presence of organic matter[2].

1. The $TiO_2$absorbs sun light in the UV range and excites an electron to the conduction band of $TiO_2$ that produce holes in valence band.

$$TiO_2 + h\nu(\lambda < 390\,nm) \rightarrow e^- + h^+ \quad (6)$$

2. The conduction band of $TiO_2$ has negative potential that reduce molecular oxygen from moisture and gets transformed into superoxide radical anion and the valence band has positive potential to generate hydroxyl radicals at the surface of $TiO_2$ while interacting with water molecules.

$$e^- + O_{2(ads)} \rightarrow .O^-_{2(ads)} \quad (7)$$

$$e^- + H^+_{(ads)} \rightarrow .H_{(ads)} \quad (8)$$

$$^+ + H_2O_{(ads)} \rightarrow H^+ + .OH_{(ads)} \quad (9)$$

The super oxide radical anion generates hydroperoxyl radical (OOH) with $H^+$ ion and promote electrochemical reduction that produces Hydrogen Peroxide causing photo degradation.

$$.O^-_{2(ads)} + H^+_{(ads)} \rightarrow HOO^- \quad (10)$$

$$HOO^- + H^+_{(ads)} \rightarrow H_2O_2 \quad (11)$$

$$H_2O_2 + h\nu \rightarrow .OH \quad (12)$$

3. The hydroxyl radical is a powerful oxidizing agent which may attack organic matter (*OM)* near or at the surface of *$TiO_2$*

$$H^+ + OM \rightarrow OM.^+ \quad (13)$$

$$.OH_{(ads)} + OM \rightarrow degradationofOM \quad (14)$$

A 5cmx 5cm of rutile phase $TiO_2$ film of undoped (UD), 2% Ca doped (D2), 3% Ca doped (D3) and 4% Ca doped (D4) were prepared using hydrothermal method. This is placed horizontally in the

mid way of dye solution whose PCA are to be measured in a beaker. After irradiation of UV light, a small portion of dye solution is taken and their respective absorbance spectra is measured. This is repeated for the time intervals of 40 min for 4 hours. Figure 10 shows the absorbance spectra of rose dye in the presence and absence of the $TiO_2$ films under different irradiation time. Also the cuvette shows the change in dye color after consecutive irradiation of UV light respectively. The peak maximum at 520 nm for anthocyanin rich dye starts decreasing on increasing the irradiation time, which shows the effect of degradation of dye in UV light. The UV light has a direct impact on the dye molecules to a smaller extent. The degradation percentage of the dye molecules is given by [47]

$$Degradation\ percentage(\%) = \frac{C_0 - C}{C_0} \quad (15)$$

Where $C_0$ and C are the initial and final concentration of dye irradiated. Figure 10 shows the UV spectra that details the degradation of rose dye by the photo electrode on irradiation. It is observed that the degradation rate of dye follows the trend: D4 > UD > D2 > D3. The photo catalytic activity of $TiO_2$ films decreases on increasing the Ca doping to 3%, but further starts increasing on 4% Ca doping. The $Ca^{2+}$ ions must have shielded the free electrons from reacting with the atmosphere. It reduces the PCA but on 4%Ca doping, the $Ca^{2+}$ ions must have intervened in the band structure of $TiO_2$ by forming trap states near the conduction band edge [48]. These traps hold the electrons excited from valence band on lower energy irradiation, which releases the electron on higher energy irradiation. This increases the number of free electrons transferred to the surface of $TiO_2$ and increase the PCA of the film compared to films UD, D2 and D3.

Under UV irradiation, the $TiO_2$ material interacts with the dye molecules and starts degrading, which is visible by its discoloration[49].Figure 11(a) shows the extent of discoloration of rose dye catalyzed by $TiO_2$ films under different irradiation time. The photo catalyzed decolorization process is described by a kinetic equation [50]

$$-ln\frac{c}{c_0^*} = k_i \times t \quad (16)$$

where $c$ is the concentration of particle at any given time, $c_0^*$ is the concentration of particle after dark adsorption, $t$ is the irradiation time and $k_i$ is the apparent kinetic constant. Figure 11 (b) shows the kinetic plot of $TiO_2$ films with different % of Ca doping. The plot gives the $R^2$ value and rate constant for the different films. The $R^2$ value determines the order of reaction. If the $R^2$>0.95, then they follow pseudo first order reaction [51]. The rate constant determines the speed of degradation of dye that takes

place by the activated catalyst film. Table 4 tabulates the parameters obtained from the linear fitting the kinetic plot of different films.

The dye molecules interact with the surface of $TiO_2$ and reduce the active sites for photocatalytic degradation[52]. This reduces the photocatalytic rate of dye molecules being degraded. Hence a consecutive cycle test was done for the rose dye with Ca doped $TiO_2$ films (D3) under UV light for five cycles as in Figure 11 (c). It is observed that the degradation percentage reduced by 5%. This interprets that the $TiO_2$ films adsorbed with higher concentration of dye molecules on the surface reduce the photocatalytic effect to an extent.

### 4.7.1. Importance of Ca doping in $TiO_2$ film

In one dimensional nanostructure, the electron movement is confined in two directions and they are free to move in one direction. This characteristic is elemental for the electron transport in the film[13]. The $TiO_2$ is intrinsically n-type with majority of electrons on the surface of the film. The band structure of $TiO_2$ nanorods are designed in such a way that the $Ti^{4+}$, 3d orbitals occupy the lower conduction band edge, whereas the $O_2^{2-}$ , 2p orbitals occupy the higher energy levels of valence band [53]. The density of states for the electrons to occupy per energy interval in the $TiO_2$ nanorod is given by

$$DOS_{1D(E)} = 2\sqrt{2}m^{\frac{1}{2}}E^{\frac{-1}{2}} \quad (17)$$

where m is the effective mass and E is the energy of electron in the $TiO_2$ lattice[54]. It can be observed that the DOS is inversely proportional to the Energy, which defines the energy levels are discrete and the higher value of DOS influences on the free states available for the electrons to occupy. The conductivity of the film depends on the efficacy of electron transport in the film, which is given by the expression.

$$\sigma = q(\mu_p p - \mu_n n) \quad (18)$$

where q is the moving carrier charge, μn and μp are the electron and hole mobilities, and n and p are the electron and hole mobile carrier concentrations, respectively[55]. The mobility of electron and holes can be increased by doping which enhance the conductivity in the film.

Doping can influence shallow /deep traps (sub bands) near the lower conduction band edge or in the upper valence band edge depending on the dopant type [56]. The electrons photo excited from the valence band are captured in the trap sites under lower exposure of radiation. These traps act as an

insulator and prevent the electron from recombination. The electron transport in the film is preceded by diffusion process through electron trapping/ detrapping mechanism [ 53]. This increases the conductivity of the film. Whereas the traps that are located deep inside the $TiO_2$, capture the electron but inhibits the mobility of electron in the film. But under high exposure of radiation, the electrons in the trap states move towards the surface of film and enhance the PCA of the film with good conduction. This provides good efficiency of DSSC for the initial exposure but after couple of minutes the dye degradation is favored which deteriorates the performance and the stability of the cell. To maintain the stability and increase the performance of DSSC, the PCA must be minimized by creating a passivation layer on the surface of $TiO_2$. To validate the above statement, we have performed doping in $TiO_2$ film to act as a passivation layer.

On doping, the dopant atomic size must be similar to $Ti^{4+}$ or $O^{2-}$ atom, so that the crystal structure of $TiO_2$ is remains unperturbed. In the present work, (1%, 2%, 3%) doping of Calcium in the $TiO_2$ matrix produces $Ca^{2+}$ ions with atomic size 0.99Å, which is larger compared to $Ti^{4+}$ ions with atomic size 0.61 Å [58]. Since the substitution of $Ca^{2+}$ instead of $Ti^{4+}$ causes distortion in the crystal lattice which affects the properties of the material, the $Ca^{2+}$ finds a suitable place on the surface of the $TiO_2$ film without disturbing the lattice. It forms surface traps on film above the conduction band level[59]. In DSSC, these surface traps may act as an insulated cavity that captures the injected electron from the dye molecules or valence band of $TiO_2$ upon excitation. These surface traps must be shielded (passivated) in such a way that the free electrons are hindered from contact with the atmosphere. Therefore, the trapped free electrons on the surface are transferred by trapping/detrapping mechanism without any loss. This might be the reason for the reduction of photo catalytic activity in the film as well as the recombination. On increasing the dopant concentration (4% Ca doped $TiO_2$), it is observed that the surface trap density linearly increases that contributes for the enhanced conduction in the film with increase in PCA[60]. The surface traps also contribute for the morphological, structural and electrical change in the film with enhanced properties. Figure 12 shows a schematic representation of PCA mechanism in undoped, 3%, and 4% Ca doped $TiO_2$nanorods sensitized by rose dye.

Another significance of doping is the enhanced surface area in the $TiO_2$ film for good dye adsorption. The $TiO_2$nanorods have good electron transfer characteristics but shows poor dye adsorption compared to $TiO_2$ nanoparticle [61]. On incorporating the foreign elements in the $TiO_2$ lattice, it acts as reactive centers favoring the dye adsorption or repellant characteristics depending on the dopant element. The $Ca^{2+}$ being a cationic dopant, it aids in dye fixation in the $TiO_2$ film. The salts of alkaline earth metals (NaCl, $CaCl_2$, and alum) are mostly used as mordants in the dye fixation in the fibre [62]. These mordants are bonded to the dye molecules by coordination complex that fasten the dye fixation and color enhancement in the fibres. Similarly the $Ca^{2+}$ ions in the $TiO_2$ film enhance the dye fixation. The enhancement in the color

and dye concentration in the sensitized $TiO_2$ film on increasing the calcium concentration shows the extent of adsorption visibly.

**4.8. Photo luminescence (PL)**

Photo luminescence is a surface phenomenon that details about the defect concentration and recombination ability of charge carriers. Figure13 shows the PL spectra for UN, D2, D3 and D4. The spectra exhibited one strong peak near UV band from 300 to 450 nm with peak maxima at 415 nm. This peak is formed as a result of near band edge UV emission of the wide band gap of $TiO_2$[63]. Another peak at 490nm corresponds to the visible emission of $TiO_2$.The $TiO_2$ absorb sunlight in the range equal to or greater than band gap energy, which excites an electron from the valence band to conduction band. The free electrons readily combine with holes forming excitons that produce a prominent peak near to UV band. But the trap states that are produced near the conduction band as result of oxygen vacancies or the interstitial defects capture these electrons and produce excitons at lower energy i.e. higher wavelength in the visible emission[63]. It can be understood that the decrease in the peak intensity in the visible region infers the minimum structural and surface defects energy levels in the $TiO_2$ films[64] [65]. This produces more free electrons on the $TiO_2$ surface to enhance conduction. This generally increases the PCA of the film as in D4. But the Ca doped films (D2, D3) passivates the electrons produced and decreases the PCA of the photo electrode to a certain extent.

.

### 4.9. Incident Photon Conversion Efficiency (IPCE)

The IPCE directly depends on the dye concentration and the electron injection efficiency of the photo electrode[66]. Figure 14 shows the IPCE spectra of UD (UV filter), UD, D2, D3 and D4 films. The IPCE spectra follow the trend in the wavelength range 400–600 nm: D3>D2>D4>UD>UD (UV Filter). The sample D3 shows the higher conversion efficiency, which can be associated with the positive shift of band gap from the UV visible absorbance spectra. 3% Ca doped nanorods (D3) has higher dye concentration and electron injection characteristics than other films that improve the photovoltaic performance of the cell. The $Ca^{2+}$ ions acts as surface traps for the electron flow and reduces the electron recombination. But the 4% Ca doped DSSC allows the electron in traps to contact with moisture enhancing the PCA resulting in degrading the IPCE efficiency. From the PCA studies, it is also evident that the dye degrades faster for D4 film, which reduces the dye concentration in the film compared to D3 on exposure to radiation. It is also evident from the IPCE results that the usage of UV filters for the undoped (UD) $TiO_2$ film in DSSC (Inset Figure), reduces the photon conversion efficiency by 10% compared to undoped (UD) DSSC. Hence passivating the PCA with Ca doped $TiO_2$ films based DSSC shows higher performance.

### 4.8. I-V studies

The photovoltaic performance of undoped and Ca-doped rose sensitized solar cells is shown in Figure 4. The inset Figure shows the IV spectra of undoped DSSC with UV filters. Table 5 shows the photovoltaic parameters including open circuit voltage (Voc), short circuit current (Jsc) , fill factor (FF) and efficiency (η) of doped and undoped DSSC with the algal buffer layers sensitized by rose dye. Compared with the undoped $TiO_2$ (UD), the Ca- doped photo electrode showed better photovoltaic performance. The fill factor of the films is also enhanced. The increase in performance of DSSC (D2, D3) is mainly ascribed to the following factors: the decrease in band gap of films that broaden the light absorbance in the visible region thereby increasing the photon conversion efficiency [67]; the introduction of nanospike structure in film enhances the light scattering; increased stability of natural dye due to passivation of PCA in the photo electrode; decrease in the valence band maximum for efficient electron injection from the dye LUMO level and higher dye concentration of the photo electrode. But the higher concentration of Ca (4%) yield lower efficiency compared D2, D3 mainly due to the coalescence of nanorods that reduce the device performance, increase in the bandgap compared D2 and D3, higher percentage of degradation of dye and lower dye concentration in the film. The use of UV filters in DSSc yields a lower $J_{sc}$ and lower $V_{oc}$ that contributes for the lower cell performance compared to undoped

(UD) DSSC. The increase in current in DSSC is mainly attributed to the large number of electron excitation from valence band to conduction band. But by using UV filters, this reduces the electronic transitions and thus the efficiency of DSSC is also lowered. Therefore in the present work Ca doping of photo electrode passivates the PCA in DSSC and yields higher performance.

## 5. Conclusions:

Ca doped $TiO_2$ nanorod structures have been successfully synthesized by one-step hydrothermal method. The effect of Ca doping into $TiO_2$ nanorods was analyzed and discussed. X-ray diffraction (XRD) measurements revealed that all the samples exhibit rutile structure. Focused Electron Scanning electron microscopy (FESEM) images revealed that the morphology of nanorods changed drastically on doping. The EDS and XPS analysis confirmed the presence of Ca in the doped $TiO_2$ films. Optical studies inferred that the band gap of the $TiO_2$ film decreased from 3.08 eV to 2.75eV on increasing the doping with Ca. Anthocyanin pigment from the rose petals was used as a sensitizer for DSSC. The PCA studies of rose dye with the Ca doped photo electrode showed a lower degradation efficiency of 30% compared to undoped $TiO_2$ photo electrode. The importance of PCA passivation in DSSC is experimented by the use of a UV filter, which showed overall lower efficiency. An effective power conversion efficiency of 2.32% was obtained for Ca (3%)-doped $TiO_2$ based DSSC as compared to undoped DSSC that exhibited an efficiency of 1.47 %. It is also observed that higher % of Ca doping leads to less adhesion of $TiO_2$ over FTO substrates.

## References

[1] G. G. G. M. N. Hemamali and G. R. A. Kumara, “Dye-Sensitized Solid State Solar Cells Sensitized with Natural Pigment Extracted from the Grapes,” vol. 3, no. 11, pp. 2–4, 2013.

[2] N. Prabavathy, S. Shalini, R. Balasundaraprabhu, D. Velauthapillai, S. Prasanna, and N. Muthukumarasamy, “Enhancement in the photostability of natural dyes for dye-sensitized solar cell (DSSC) applications: a review,” *Int. J. Energy Res.*, 2017.

[3] C. Ravidhas *et al.*, “Tunable morphology with selective faceted growth of visible light active TiO2

thin films by facile hydrothermal method: structural, optical and photocatalytic properties," *J. Mater. Sci. Mater. Electron.*, 2016.

[4] A. Zyoud *et al.*, "Alternative natural dyes in water puri fi cation : Anthocyanin as TiO 2 -sensitizer in methyl orange photo-degradation," vol. 13, pp. 1268–1275, 2011.

[5] M. Carnie, T. Watson, and D. Worsley, "UV Filtering of Dye-Sensitized Solar Cells : The Effects of Varying the UV Cut-Off upon Cell Performance and Incident Photon-to-Electron Conversion Efficiency," vol. 2012, 2012.

[6] R. Syafinar, N. Gomesh, M. Irwanto, M. Fareq, and Y. M. Irwan, "Optical characterization using nature based dye extracted from hibiscus's flower," *ARPN J. Eng. Appl. Sci.*, vol. 10, no. 15, pp. 6336–6340, 2015.

[7] N. P. S. Shalini and R. B. Dhayalan, "Effect of solvents in the extraction and stability of anthocyanin from the petals of Caesalpinia pulcherrima for natural dye sensitized solar cell applications," *J. Mater. Sci. Mater. Electron.*, vol. 0, no. 0, p. 0, 2017.

[8] K. Srikanth *et al.*, "Investigation of the effect of sol processing parameters on the photoelectrical properties of dye-sensitized TiO2 solar cells," *Sol. Energy Mater. Sol. Cells*, vol. 65, pp. 171–177, 2001.

[9] J.-K. Oh, J.-K. Lee, H.-S. Kim, S.-B. Han, and K.-W. Park, "TiO $_2$ Branched Nanostructure Electrodes Synthesized by Seeding Method for Dye-Sensitized Solar Cells $^{\dagger}$," *Chem. Mater.*, vol. 22, no. 3, pp. 1114–1118, 2010.

[10] S. Kathirvel, C. Su, H.-C. Lin, B.-R. Chen, and W.-R. Li, "Facile non-hydrolytic solvothermal synthesis of one dimensional TiO2 nanorods for efficient dye-sensitized solar cells," *Mater. Lett.*, vol. 129, pp. 149–152, 2014.

[11] H. Wang *et al.*, "Multifunctional TiO2 nanowires-modified nanoparticles bilayer film for 3D dye-sensitized solar cells," *Optoelectron. Adv. Mater. Rapid Commun.*, vol. 4, no. 8, pp. 1166–1169, 2010.

[12] J. Rouhi, M. H. Mamat, C. H. R. Ooi, S. Mahmud, and M. R. Mahmood, "High-performance dye-sensitized solar cells based on morphology-controllable synthesis of ZnO-ZnS heterostructure nanocone photoanodes," *PLoS One*, vol. 10, no. 4, pp. 1–14, 2015.

[13] J. Qu and C. Lai, "One-dimensional TiO 2 nanostructures as photoanodes for dye-sensitized solar

cells," *J. Nanomater.*, vol. 2013, p. 2, 2013.

[14] Z. Lan, X. Chen, S. Zhang, and J. Wu, "CdSe x S 1 − x / CdS-cosensitized 3D TiO 2 hierarchical nanostructures for efficient energy conversion," pp. 1–7, 2017.

[15] X. Chen, S. S. Mao, X. Chen, and S. S. Mao, "Titanium Dioxide Nanomaterials : Synthesis , Properties , Modifications , and Applications Titanium Dioxide Nanomaterials : Synthesis , Properties , Modifications , and Applications," vol. 107, no. June, pp. 2891–2959, 2007.

[16] Z. R. Ismagilov, L. T. Tsikoza, N. V Shikina, V. F. Zarytova, V. V Zinoviev, and S. N. Zagrebelnyi, "Synthesis and stabilization of nano-sized titanium dioxide," *Russ. Chem. Rev.*, vol. 78, no. 9, pp. 873–885, 2009.

[17] M. Malekshahi Byranvand, A. N. Kharat, L. Fatholahi, and Z. M. Beiranvand, "A Review on Synthesis of Nano-TiO 2 via Different Methods," *Jns*, vol. 3, pp. 1–9, 2013.

[18] X. Chen, Z. Lan, S. Zhang, J. Wu, and J. Zhang, "CdS sensitized TiO 2 nanorod arrays based solar cells prepared with polymer-assisted layer-by-layer adsorption and reaction method," *Opt. Commun.*, pp. 1–6, 2016.

[19] L. G. Devi, B. N. Murthy, and S. G. Kumar, "Photocatalytic activity of TiO2 doped with Zn2+ and V5+ transition metal ions: Influence of crystallite size and dopant electronic configuration on photocatalytic activity," *Mater. Sci. Eng. B Solid-State Mater. Adv. Technol.*, vol. 166, no. 1, pp. 1–6, 2010.

[20] W. Li, J. Yang, J. Zhang, S. Gao, Y. Luo, and M. Liu, "Improve photovoltaic performance of titanium dioxide nanorods based dye-sensitized solar cells by Ca-doping," *Elsevier Ltd*, vol. 57, pp. 177–183, 2014.

[21] N. Prabavathy *et al.*, "Algal buffer layers for enhancing the efficiency of anthocyanins extracted from rose petals for natural dye-sensitized solar cell (DSSC)," *Int. J. Energy Res.*, no. July, pp. 1–12, 2017.

[22] Y. Li, M. Guo, M. Zhang, and X. Wang, "Hydrothermal synthesis and characterization of TiO2 nanorod arrays on glass substrates," *Mater. Res. Bull.*, vol. 44, pp. 1232–1237, 2009.

[23] Y. Akila, N. Muthukumarasamy, S. Agilan, T. K. Mallick, S. Senthilarasu, and D. Velauthapillai, "Enhanced performance of natural dye sensitised solar cells fabricated using rutile TIO2 nanorods," *Opt. Mater. (Amst).*, vol. 58, pp. 76–83, 2016.

[24] A. Subramanian and H.-W. Wang, "Effects of boron doping in TiO2 nanotubes and the performance of dye-sensitized solar cells," *Appl. Surf. Sci.*, vol. 258, no. 17, pp. 6479–6484, 2012.

[25] A. Kumar and P. Agarwal, "Application of natural dyes on textiles," vol. 34, no. December, pp. 384–399, 2009.

[26] A. N. Banerjee, "The design , fabrication , and photocatalytic utility of nanostructured semiconductors : focus on TiO 2 -based nanostructures," pp. 35–65, 2011.

[27] Y. H. Jung, K.-H. Park, J. S. Oh, D.-H. Kim, and C. K. Hong, "Effect of TiO2 rutile nanorods on the photoelectrodes of dye-sensitized solar cells.," *Nanoscale Res. Lett.*, vol. 8, no. 1, p. 37, 2013.

[28] S. Shalini *et al.*, "Effect of Na doping on structure, morphology and properties of hydrothermally grown one dimensional TiO2 nanorod structures," *J. Mater. Sci. Mater. Electron.*, 2016.

[29] S. Chen and J. Wu, "Nucleation mechanisms and their influences on characteristics of ZnO nanorod arrays prepared by a hydrothermal method," *Acta Mater.*, vol. 59, no. 2, pp. 841–847, 2011.

[30] A. Thapa, J. Zai, H. Elbohy, P. Poudel, N. Adhikari, and X. Qian, "TiO 2 Coated Urchin-like SnO 2 Microspheres for Efficient Dye-Sensitized Solar Cells TiO 2 Coated Urchin-like SnO 2 Microspheres for Efficient Dye-Sensitized Solar Cells," 2014.

[31] S. S. Mali, C. A. Betty, P. N. Bhosale, P. S. Patil, and C. K. Hong, "From nanocorals to nanorods to nanoflowers nanoarchitecture for efficient dye-sensitized solar cells at relatively low film thickness: All Hydrothermal Process," *Sci. Rep.*, vol. 4, pp. 2–9, 2014.

[32] M. Singh, M. Goyal, and K. Devlal, "Size and shape effects on the band gap of semiconductor compound nanomaterials," *J. Taibah Univ. Sci.*, vol. 0, no. 0, pp. 1–6, 2018.

[33] J. O. F. S. Sciencetechnology, "Solanum nigrum and Eclipta alba leaf pigments for dye sensitized solar cell applications," no. JANUARY 2014, pp. 13–17, 2015.

[34] Y. Akila, N. Muthukumarasamy, S. Agilan, S. Senthilarasu, and D. Velauthapillai, "Zirconium oxide post treated tin doped TiO2 for dye sensitized solar cells," *Mater. Sci. Semicond. Process.*, vol. 57, no. September 2016, pp. 24–31, 2017.

[35] Y. Paz, "Self-assembled monolayers and titanium dioxide: From surface patterning to potential applications," *Beilstein J. Nanotechnol.*, vol. 2, no. 1, pp. 845–861, 2011.

[36] P. Babelon, A. S. Dequiedt, H. Mostefa-Sba, S. Bourgeois, P. Sibillot, and M. Sacilotti, "SEM and XPS studies of titanium dioxide thin films grown by MOCVD," *Thin Solid Films*, vol. 322, no. 1–2, pp. 63–67, 1998.

[37] K. Hwang, S. Yoo, S. Jung, D. Park, S. Kim, and J. Lee, "Synthesis and Characterization of Nanostructured Titania Films for Dye-Sensitized Solar Cells," *Adsorpt. J. Int. Adsorpt. Soc.*, vol. 30, no. 1, pp. 172–176, 2009.

[38] I. Jang, K. Song, J. H. Park, and S. G. Oh, "Enhancement of dye adsorption on TiO2 surface through hydroxylation process for Dye-sensitized solar cells," *Bull. Korean Chem. Soc.*, vol. 34, no. 10, pp. 2883–2888, 2013.

[39] A. O. T. Patrocinio, E. B. Paniago, R. M. Paniago, and N. Y. Murakami Iha, "XPS characterization of sensitized n-TiO2 thin films for dye-sensitized solar cell applications," *Appl. Surf. Sci.*, vol. 254, pp. 1874–1879, 2008.

[40] S. a. Pawar *et al.*, "Hydrothermal growth of photoelectrochemically active titanium dioxide cauliflower-like nanostructures," *Electrochim. Acta*, vol. 117, pp. 470–479, 2014.

[41] G. Balaji, R. Balasundaraprabhu, S. Prasanna, N. Prabavathy, D. N. McIlroy, and M. D. Kannan, "Investigations of RF magnetron sputtered CZTS absorber layer thin films prepared using sulfur induced binary targets without sulfurization," *Opt. Mater. (Amst).*, vol. 75, pp. 56–60, 2018.

[42] H. Fan *et al.*, "Band alignment of TiO2 / FTO interface determined by X-ray photoelectron spectroscopy : Effect of annealing Band alignment of TiO 2 / FTO interface determined by X-ray photoelectron spectroscopy : Effect of annealing," vol. 15314, 2016.

[43] V. Pfeifer *et al.*, "Energy Band Alignment between Anatase and Rutile TiO 2," 2013.

[44] A. R. Khataee and M. B. Kasiri, "Photocatalytic degradation of organic dyes in the presence of nanostructured titanium dioxide: Influence of the chemical structure of dyes," *J. Mol. Catal. A Chem.*, vol. 328, no. 1–2, pp. 8–26, 2010.

[45] O. Sacco, M. Stoller, V. Vaiano, P. Ciambelli, A. Chianese, and D. Sannino, "Photocatalytic degradation of organic dyes under visible light on n-doped TiO2 photocatalysts," *Int. J. Photoenergy*, vol. 2012, 2012.

[46] H. S. Jung *et al.*, "Mobility enhanced photoactivity in sol-gel grown epitaxial anatase TiO 2 films," *Langmuir*, vol. 24, no. 6, pp. 2695–2698, 2008.

[47] V. Madurai, M. Natarajan, A. Santhanam, V. Asokan, and D. Velauthapillai, "Size controlled synthesis of TiO 2 nanoparticles by modi fi ed solvothermal method towards e ff ective photo catalytic and photovoltaic applications," vol. 97, no. September 2017, pp. 351–360, 2018.

[48] Y. C. Lee, Y. J. Jung, and P. Y. Park, "Increase the efficiency of dye-sensitized TiO 2 solar cell ( DSSC ) by doping on TiO 2 semiconductor," *Mater. Sci.*, pp. 2003–2003, 2003.

[49] M. Anas, D. Suk, K. Mahmoud, H. Park, and A. Abdel-wahab, "Materials Science in Semiconductor Processing Photocatalytic degradation of organic dye using titanium dioxide modi fi ed with metal and non-metal deposition," *Mater. Sci. Semicond. Process.*, vol. 41, pp. 209–218, 2016.

[50] R. S. Sonawane, B. B. Kale, and M. K. Dongare, "Preparation and photo-catalytic activity of Fe – TiO 2 thin films prepared by sol – gel dip coating," vol. 85, no. 3, pp. 52–57, 2004.

[51] F. Akbal, "Photocatalytic Degradation of Organic Dyes in the Presence of Titanium Dioxide under UV and Solar Light : Effect of Operational," vol. 24, no. 3, pp. 317–322, 2005.

[52] N. B. Gusiak, I. M. Kobasa, and S. S. Kurek, "Nature inspired dyes for the sensitization of titanium dioxide photocatalyst," *Chemik*, vol. 67, no. 12, pp. 1191–1198, 2013.

[53] X. Wang, Z. Li, J. Shi, and Y. Yu, "One-Dimensional Titanium Dioxide Nanomaterials : Nanowires ," 2014.

[54] H. S. Kim, Y. J. Kim, W. Lee, and S. H. Kang, "One-pot synthesis of peacock-shaped TiO2 light scattering layer with TiO2 nanorods film for dye-sensitized solar cells," *Appl. Surf. Sci.*, vol. 273, pp. 226–232, 2013.

[55] A. M. Bakhshayesh and M. R. Mohammadi, "The improvement of electron transport rate of TiO2 dye-sensitized solar cells using mixed nanostructures with different phase compositions," *Ceram. Int.*, vol. 39, no. 7, pp. 7343–7353, 2013.

[56] B. Roose, "Chem Soc Rev," 2015.

[57] J. R. Jennings, A. Ghicov, L. M. Peter, P. Schmuki, and A. B. Walker, "Dye-sensitized solar cells based on oriented TiO2 nanotube arrays: transport, trapping, and transfer of electrons.," *J. Am. Chem. Soc.*, vol. 130, no. 40, pp. 13364–72, Oct. 2008.

[58] M. Motlak *et al.*, "Dye-Sensitized Solar Cells Using Novel," vol. 2, no. 3, pp. 217–221, 2013.

[59] J. Zhang, J. Feng, Y. Hong, Y. Zhu, and L. Han, "Effect of different trap states on the electron transport of photoanodes in dye sensitized solar cells," *J. Power Sources*, vol. 257, pp. 264–271, 2014.

[60] M. J. Cass, A. B. Walker, D. Martinez, and L. M. Peter, "Grain morphology and trapping effects on electron transport in dye-sensitized nanocrystalline solar cells.," *J. Phys. Chem. B*, vol. 109, no. 11, pp. 5100–7, Mar. 2005.

[61] L. Dong *et al.*, "Hydrothermal growth of rutile TiO2 nanorod films on titanium substrates," *Thin Solid Films*, vol. 519, no. 15, pp. 4634–4640, 2011.

[62] M. Sci, M. E. Doi, S. Science, B. Media, and N. York, "Effects of Na-doping on the efficiency of ZnO nanorods-based dye sensitized solar cells," vol. 2, 2014.

[63] X. Wang, Z. Feng, J. Shi, G. Jia, and S. Shen, "Trap states and carrier dynamics of TiO 2 studied by photoluminescence spectroscopy under weak excitation condition," pp. 7083–7090, 2010.

[64] C. Jin, B. Liu, Z. Lei, and J. Sun, "Structure and photoluminescence of the TiO2 films grown by atomic layer deposition using tetrakis-dimethylamino titanium and ozone," *Nanoscale Res. Lett.*, vol. 10, no. 1, 2015.

[65] L. Que, Z. Lan, W. Wu, J. Wu, J. Lin, and M. Huang, "High-ef fi ciency dye-sensitized solar cells based on ultra-long single crystalline titanium dioxide nanowires," *J. Power Sources*, vol. 266, pp. 440–447, 2014.

[66] R. Kushwaha, P. Srivastava, and L. Bahadur, "Natural Pigments from Plants Used as Sensitizers for TiO 2 Based Dye-Sensitized Solar Cells," *J. Energy*, vol. 2013, no. Ii, 2013.

[67] N. Gokilamani, N. Muthukumarasamy, M. Thambidurai, A. Ranjitha, and D. Velauthapillai, "Utilization of natural anthocyanin pigments as photosensitizers for dye-sensitized solar cells," *Journal of Sol-Gel Science and Technology*, vol. 66, no. 2. pp. 212–219, 2013.

**Figure 1: XRD Spectra of undoped and Ca- doped $TiO_2$ films**

**Figure 2: TEM images and SAED pattern of (a,b,c) undoped $TiO_2$ film (UD) ; (d,e,f) Ca doped $TiO_2$ film (D3)**

**Figure 3: a,b,c) Undoped $TiO_2$nanorod (UD); d,e,f) 1% Ca-doped $TiO_2$nanorods (D1) ; g, h, i) 2% Ca-doped $TiO_2$ nanorods (D2) ; j, k, l) 3% Ca-doped $TiO_2$ nanorods (D3); m,n,o) 4% Ca doped $TiO_2$ nanorods (D4) and their corresponding cross sectional images.**

**Figure 4: Representation of Morphological changes in $TiO_2$ film because of Ca doping.**

**Figure 5: EDAX analysis and mapping of a,b,c,d) undoped $TiO_2$ nanorod (UD); and e,f,g,h,i) 3% Ca doped $TiO_2$ nanorod (D3).**

**Figure 6: a) Tauc plot of $TiO_2$ thin films (Inset Figure: Absorbance spectra of $TiO_2$ films); b) Absorbance spectra of rose sensitized $TiO_2$ films with algal buffer layers.**

**Figure 7: (a) Survey Spectrum of undoped (UD) and Ca doped (D3) $TiO_2$ films; (b) Core Level spectra of Ti in samples UD and D3; (c) Core level spectra Ca in D3; (d) Core level spectra of O in UD and D3;(e) Deconvolution of O1s in the UD thin film.**

**Figure 8: (a) Valence Band (VB) spectra of films UD and D3; (b) Representation of band diagram of films UD and D3 for effective electron injection from the dye molecules sensitized.**

**Figure 9: PCA of $TiO_2$ particles in presence of sunlight** [2]

**Figure 10: Effect of dye degradation in presence of $TiO_2$ films (UD, D2, D3, and D4) under UV light for an interval of 40 mins for 4 hrs.**

**Figure 11: (a) Degradation efficiency of rose dye in presence of UD, D2 , D3 and D4; (b) Kinetic plots of UD, D2 , D3 and D4; (c) Cycle test for repeatability of D3 film**

**Figure 12: Schematic representation of PCA mechanism in undoped and 3%, 4%Ca doped $TiO_2$nanorods sensitized by natural dye: 1.Sunlight is irradiated on natural dye sensitized $TiO_2$ film that enters the valence band of $TiO_2$ molecules and natural dye molecules. 2. This cause electron excitation from CB to VB and dye excitation from HOMO to LUMO level respectively; 3.Electron is injected from LUMO of the dye molecules to CB of $TiO_2$; 4. The moisture in the atmosphere reacts with the free electrons on the surface of $TiO_2$ film and produces superoxide and hydroxyl free radicals; 5.The free radicals destroys the dye molecules on the surface of $TiO_2$ film; 6.The free**

**electrons generated from Valence Band and dye molecules are captured by $Ca^{2+}$ atoms that act as surface traps in Ca doped $TiO_2$ films; 7. The free electrons captured by traps are hence passivated from the atmosphere and transported along the film by diffusion mechanism; 8. The increase in Ca concentration leads to shallow traps that releases electrons passivated by Ca dopant and increase the PCA in DSSC.**

**Figure 13: PL spectra of undoped and Ca- doped $TiO_2$ films**

**Figure 14: IPCE spectra of undoped and Ca- doped DSSC. (Inset figure – IPCE spectra of undoped DSSC in presence of UV filter).**

**Figure 15: IV characteristics of undoped and Ca-doped DSSC. (Inset figure – IV spectra of undoped (UD) DSSC in presence of UV filter).**

**Table 1: Crystallite size and strain parameters of the undoped and Ca doped $TiO_2$ films**

| Film | Average Crystallite Size (nm) | Strain |
|---|---|---|
| **UD** | 31.43 | 0.00131 |
| **D1** | 31.85 | 0.00132 |
| **D2** | 32.23 | 0.00131 |
| **D3** | 32.44 | 0.00133 |
| **D4** | 31.12 | 0.00166 |

**Table 2: Dye concentration in rose sensitized undoped and doped $TiO_2$ nanorods**

| Sample with algal buffer layers | Dye adsorption ($\times 10^{-8}$ mol $cm^{-2}$) |
|---|---|
| Rose sensitized Undoped $TiO_2$nanorods | 4.52 |

| | |
|---|---|
| Rose sensitized 1% Ca doped $TiO_2$nanorods | 5.50 |
| Rose sensitized 2% Ca doped $TiO_2$nanorods | 6.38 |
| Rose sensitized 3% Ca doped $TiO_2$nanorods | 8.14 |
| Rose sensitized 4% Ca doped $TiO_2$nanorods | 4.82 |

**Table 3: Composition of individual elements present in UD and D3 thin films**.

| Films | Annealing Temperature (°C) | Ti % | O % | Ca % |
|---|---|---|---|---|
| UD | 450 | 34.2 | 57.8 | - |
| D3 | 450 | 31.9 | 54.8 | 4.3 |

**Table 4: Parameters obtained from the kinetic plot of UD, D2, D3 and D4 with degradation rate**

| Films | $R^2$ | K | Degradation rate (%) |
|---|---|---|---|
| **UD** | 0.98 | 0.236 | 73 |
| **D2** | 0.96 | 0.120 | 60 |
| **D3** | 0.95 | 0.158 | 45 |
| **D4** | 0.99 | 0.224 | 68 |

**Table 5: Photovoltaic parameters of Ca- doped and undoped DSSC with rose as sensitizer and inclusive of algal buffer layers.**

| $TiO_2$ based solar cell | $J_{sc}$ (mA/cm$^2$) | $V_{oc}$ (V) | FF | η (%) |
|---|---|---|---|---|
| ***Undoped DSSC (UD with UV Filter)*** | 4.8 | 0.55 | 0.57 | 1.26 |
| ***Undoped DSSC (UD)*** | 5.8 | 0.60 | 0.41 | 1.47 Previous work [21] |

| | | | | |
|---|---|---|---|---|
| ***2% Ca doped DSSC (D2)*** | 7.0 | 0.63 | 0.60 | 1.94 |
| ***3% Ca doped DSSC (D3)*** | 7.3 | 0.63 | 0.69 | 2.32 |
| ***4% Ca doped DSSC (D4)*** | 6.6 | 0.59 | 0.47 | 1.60 |